Biomolecular Mode of Action of Metformin in Relation to Its Copper Binding Properties

The Bio-Molecular Mode of Action of Metformin in Relation to its Copper Binding Properties

*Peter Repiščák[†], Stefan Erhardt[†], Graham Rena[‡] and Martin J. Paterson[†]**

[†]Institute Of Chemical Sciences, School of Engineering and Physical Sciences, Heriot-Watt University, Edinburgh, United Kingdom EH14 4AS

[‡]Cardiovascular and Diabetes Medicine, Ninewells Hospital and Medical School, University of Dundee, Dundee, United Kingdom, DD1 9SY

Funding Sources

MJP and PR thank the European Research Council for funding under the European Union's Seventh Framework Programme (FP7/2007-2013)/ERC Grant No. 258990. MJP and SE thank the Leverhulme Trust for funding through a research grant RPG-165. GR acknowledges support from MRC and Diabetes UK.

***Corresponding Author:**

Phone: +44(0)131 451 8035. E-mail: m.j.paterson@hw.ac.uk

ABBREVIATIONS

AMP, 5' adenosine monophosphate; AMPK, AMP-activated protein kinase; AO, atomic orbital; B3LYP, Becke-3-Lee-Yang-Parr density functional; BG, biguanide; BG-H, deprotonated biguanide; CSD, Cambridge Structural Database; DFT, density functional theory; en, ethylenediamine; ESP, electrostatic potential; MO, molecular orbital; Metf, metformin N,N-dimethylbiguanide; Metf-H, deprotonated metformin; NBO, natural bond orbital; PDI, propanediimidamide; T2D, type 2 diabetes; trien, triethylenetetramine.

KEYWORDS

Type 2 diabetes; metformin; structure activity relationship; pharmacology; copper binding; computational chemistry; DFT

ABSTRACT

Metformin (Metf), the most commonly used type 2 diabetes drug, is known to affect the cellular housekeeping of copper. Recently we discovered that the structurally closely related propanediimidamide (PDI) shows a different cellular behaviour than metformin. Here we investigate the binding of these compounds to copper, to compare their binding strength. Furthermore we take a closer look at the electronic properties of these compounds and their copper complexes such as molecular orbital interactions and electrostatic potential surfaces. Our results clearly show that the copper binding energies cannot alone be the cause for the biochemical differentiation between Metf and PDI. We conclude that other factors such as pK_a values and hydrophilicity of the compounds play a crucial role in their cellular activity. Metf in contrast to PDI can occur as an anion in aqueous medium at moderate pH, forming much stronger complexes particularly with Cu^{II} ions, suggesting that biguanides but not PDI may induce easy oxidation of Cu^{I} ions extracted from proteins. The higher hydrophobicity and lack of planarity of PDI may further differentiate it from biguanides in terms of their molecular recognition characteristics. These different properties could hold the key to metformin's mitochondrial activity because they suggest that the drug could act at least in part as a pro-oxidant of accessible protein-bound Cu^{I} ions.

INTRODUCTION

It has been estimated that more than 300 million people suffer from the diabetes world-wide.[1] By 2030 the WHO estimates that diabetes will be the seventh highest cause of death.[2] Type 2 diabetes (T2D), which covers around 90% of all diabetes patients, is characterised by hyperglycaemia due to insulin resistance in peripheral tissues. One of the most effective and frequently administered antihyperglycemic T2D drugs is metformin (N,N-dimethylbiguanide, Metf; for its chemical structure see Figure 1), which is the first-line treatment because of better long-term outcomes compared with other therapies such as insulin secretagogues.[3] It belongs to the biguanide family that also include other compounds with antihyperglycemic properties. Metf and other biguanide derivatives have been developed after it was discovered that the blood glucose-lowering ingredient in Goat's Rue is guanidine and other guanidine derivatives such as galegine. Synthalin, a diguanide, was developed as a synthetic drug and was more potent and showed lower toxicity. However, the liver damage caused by both guanidine and diguanides, were a stimulant to search for safer alternatives which led to the development of biguanides as T2D drugs.[3]

The exact molecular mechanism of Metf and other T2D drugs remains unclear. One suggested mechanism of action is suppression of mitochondrial respiration by inhibition of complex I[4, 5], however, the precise mechanism of this inhibition has not yet been established.

Dysfunctional copper metabolism is implicated in the development of several diseases. [6-9] Mutations in the gene ATP7A results in copper deficiency in most organs, which is the cause of Menkes's disease[10, 11] and copper overload resulting from ATP7B mutation is the cause of Wilson's disease.[12] Dysregulation of copper is also suspected in other diseases, particularly those involving protein misfolding[13-15] and in diabetes.[16-20]

In our previous study we demonstrated for the first time that the metal-binding properties of Metf, particularly towards copper, may be one factor in cell responses to this drug.[21] Metf and biguanide (BG) show antihyperglycemic properties and no free mitochondrial Cu^{II} could be detected by a Cu^{II} specific fluorescence probe. In contrast propanediimidamide (PDI) showed no antihyperglycemic effect and free Cu^{II} was detected. BG and Metf regulate AMP-activated protein kinase (AMPK), whereas PDI does not have such an effect. Regulation of S6 phosphorylation is observed for all three compounds. Interestingly, Metf does not lower the urinal copper concentration which in T2D patients is raised, whereas triethylenetetramine (trien) decreases the urinal copper concentration, but has no antihyperglycemic effect.

FIGURE 1

However, it remained unclear whether Metf binds to Cu^{I} or Cu^{II}. In water Cu^{II} is the more stable oxidation state. In living organisms a complex machinery of cupric reductase, a Cu^{I} specific membrane transport protein, and chaperone proteins within the cells exist which effectively does not allow free copper ions at cellular level.[22-29] The chaperone proteins play a vital role in the copper transport system and are not only abundant in the cell but also in the mitochondria. Cu^{I} is bound to the chaperones by two cysteinates. At the unbound state these cysteines are protonated, therefore, a perfectly designed proton array consisting of other amino acids is constructed to deprotonate the receiving chaperones or enzymes while simultaneously protonating the transporter protein to lower its copper binding affinity. Moreover, copper metalloenzymes, where the unique copper redox chemistry is needed, are able to bind both Cu^{I}

and Cu^{II}. Therefore, there are various possibilities of drug interaction with $Cu^{I/II}$ proteins and Metf could potentially interact with protein bound $Cu^{I/II}$ ions.

There are major differences in the coordination chemistry of Cu^{I} and Cu^{II}. At the lower oxidation state Cu^{I} prefers binding to soft ligands such as thiols, thiolates (cysteine) or thioethers (methionine) or sp^2 containing nitrogen (histidine). On the other hand, Cu^{II} favours binding to slightly harder ligands such as amines and imines. According to Pearson's hard and soft acids and bases (HSAB) concept Cu^{I} is classified as a soft acid whereas Cu^{II} is classified as an intermediate acid.[30-33] Also Cu^{I} has 2-4 ligand atoms in the first coordination sphere compared to 3-6 for Cu^{II}. Generally a tetrahedral coordination sphere is observed for Cu^{I}, whereas a square planar ligand orientation is commonly found for Cu^{II}.[34,35] In an enzymatic environment a mixed coordination sphere of sulphur and nitrogen containing ligands assist to stabilise Cu^{I} and at the same time facilitates the reversible redox chemistry of $Cu^{I/II}$.

Similar to the imidazole residue in histidine a sp^2 hybridised N1 (for atom labels see Figure 2) is the ligand atom for BG, Metf and PDI. This means that π-backbonding can occur and stabilize the lower Cu^{I} oxidation state by transferring electron density into the π-orbitals of the ligands, see Figure 3. This type of molecular orbital (MO) interaction may also be important for Cu^{II} as its 3d-orbitals are almost filled up. The methylene CH_2 moiety in PDI compared to the secondary amine N2 in BG and Metf causes a disruption of the π-system, whereas the lone-pair of N2 can contribute electron density into the adjacent carbon p_z-orbital in BG and Metf, which results in a planar molecular structure for the latter ones and a non planar geometry for PDI in the complex. This is similar to the stabilisation effect detected in peptide bonds.

FIGURE 2

FIGURE 3

Additionally, the N2-H group contains a protic hydrogen whereas the methylene hydrogens cannot undergo proton exchange in aqueous media. Deprotonated metal complexes of PDI are known, however, those are synthesised in non-protic solvents under conditions that avoid any water contamination.[36-38] Due to the protic hydrogen the most stable neutral form of BG and Metf in water is a tautomer in which the N2-H proton is formally transferred to N1 or N3.[39] This leads to a fully conjugated π-system in the ligands. However, only the N2 can then act as a donor atom as has been observed with a similar ligand in a known Ag^{I} complex.[40]

Biguanides formally belong to the 1,3,5-triazapentadienyl[41, 42] (also known as imidoylamidine) ligand family and PDI is a member of the 1,5-diazapentadienyl[35, 38, 43] (also known as β-diketiminate) ligand class which are well established as metal ion ligands in inorganic coordination chemistry. However, their structure and chemistry is mainly established in nonaqueous solvents, hence, their properties cannot be transferred directly to aqueous environments particularly biosystems with very sensitive pH range.

The protonation equilibria of BG have been studied along with complex formation with Cu^{II} at a pH range of 2-12.[44, 45] Firstly, BG predominately exists in an equilibrium between its monoprotonated and neutral form at physiological pH and no deprotonated BG-H was reported for the given pH range. Secondly, the formation of $[Cu^{II}(OH)(BG)]^{+}$ was observed to be the major Cu-BG complex, however, binary Cu^{II}-BG complexes such as $[Cu(BG)_2]^{2+}$, $[Cu(BG)(BG\text{-}H)]^{+}$ and $[Cu(BG\text{-}H)_2]^{0}$ were also observed at slightly higher pH values. The pKa value of 6.88 was reported for $[Cu(OH)(BG)]^{+}$ hence indicating the possibility of deprotonated BG while being

coordinated to Cu^{II}. Neither Metf nor PDI have been studied in this detail. However, these results are at least qualitatively transferable to Metf.

In a recent study the antimicrobial properties of binary metformin metal complexes were studied.[46,47] Among other physico-chemical properties the cyclic voltammogram of $[Cu^{II}(Metf)_2]^{2+}$ was measured against a Ag/AgCl electrode and showed a reduction peak at 320mV and oxidation peak at 490mV giving a $E_{1/2}$ of +405 mV which is in the range of the reduction potentials of copper containing enzymes.[48]

Here we aim to build upon our previous work on the cellular response to T2D drugs and in particular on the observed variations of free copper levels after drug treatment. We gain deeper insight into the copper binding properties of BG and Metf with focus on possible differences to PDI**,** which may be important for their different biological antihyperglycemic properties. We compute binding energies and compare the optimized structures to known crystal structures, in the process benchmarking the computational methodology for such systems. Furthermore we will investigate the electronic properties such as molecular orbitals and electrostatic potentials of these molecules.

MATERIALS AND METHODS

Computational Details

Geometries of all the computed structures were obtained by optimization with B3LYP[49-53]. The basis set Def2-TZVPD[54] was used for all atoms. For Cu(I) complexes singlet spin-multiplicity was used, while for Cu(II) doublet spin-multiplicity was used. For the open-shell species spin-contamination was found to be negligible. Each structure was verified to be a minimum by the absence of imaginary frequencies in the vibrational analysis. The calculations were performed

using Gaussian 09 A.02 and C.01[55]. We also tested other DFT functionals including BP86[51, 56], M06[57] and M06L[58] which showed no significant difference to B3LYP. Natural bond orbital (NBO) charges were calculated with the integrated NBO 3.1[59] within Gaussian 09.

RESULTS

A. Comparision of X-ray Structures and Computed Complexes

Several crystal structures are known for bisbiguanide-copper complexes. Three describe the $[Cu(BG)_2]^{2+}$ complex and contain different counterions.[60-62] Although these complexes are planar they are not symmetric in terms of their bond lengths. An average over all three structures is presented in Table 1 and will be discussed here in comparison to the DFT optimized structure. One structure for the neutral complex $Cu(BG\text{-}H)_2$[63] has been published which contains the deprotonated biguanide (BG-H). The deprotonation was confirmed by visual inspection of H-bond contacts to the deprotonated N2(-).

The observed Cu-N1 bond length 1.944 Å is in the normal range of Cu^{II}-N ligand bonds. The computed Cu-N bond distance 1.980 Å is slightly longer, however, this is expected and is a known effect when computing complexes in gas phase and comparing them to crystal structures. Also the Cu-N bond length in the different crystal structures can vary from 1.921 Å to 1.958 Å for complexes with the neutral BG ligand. The most symmetrical, coplanar X-ray structure COBMAH[61] is C_i symmetric with Cu-N distances of 1.933 and 1.939 Å. This feature is reproduced by the DFT calculation with slightly different Cu-N bonds of 1.978 and 1.982 Å. Interestingly, the computed minimum structure is slightly twisted and has C_2 symmetry with regards to the heavy atoms which is abolished by the non-planar H-atoms of the amine groups.

The coplanar, D_{2h} symmetrical geometry is in fact computed to be a rotational transition state in the gas phase with a negligible barrier of $\Delta E^{\ddagger}$ 1.04 and $\Delta G^{\ddagger}$ 3.65 kcal/mol.

The observed N1-C1 bond length (X-ray_{av}: 1.292 Å; DFT: 1.299 Å) is slightly longer than a pure C-N double bond and whereas the C1-N2 (X-ray_{av}: 1.373 Å; DFT: 1.383 Å) and C1-N3 (X-ray_{av}: 1.343 Å; DFT: 1.344 Å) are much shorter than a C-N single bond, which indicates conjugation of the N2-lone pairs into the N1-C1 double bound. The computed N-C bonds are in much better agreement with the crystal structure compared to the metal-ligand bond because these bonds are less affected by crystal packing. Particularly the changes upon deprotonation of the secondary amine N2-H in the N1-C1 and C1-N2 bonds which indicate a delocalization of the negative charge within the ligand bonds that form the metallacycle is very well reproduced in the computed structure. The observed differences between the different X-ray structures are possibly explained by the different counter ions. Remarkably, an almost negligible shortening of -0.002 Å for the Cu-N bond length is observed for the neutral complex $Cu(BG\text{-}H)_2$[63] compared to the average of the cationic complexes, whereas the DFT calculations reveal a stronger reduction of -0.009 Å indicating a much larger increase in the Cu-N bond strength than the experimental results are suggesting.

TABLE 1

Moving on to the Metf-Cu complexes, in total five crystal structures are known, see Table 2, three include the neutral Metf[47, 64, 65] and two the deprotonated metformin (Metf-H)[64, 65] with Cu^{II}. Some differences compared to the BG-Cu complexes in the bond distances can be observed which are due to the methyl groups that abolish the symmetry of the BG complex. The N1-C1

bond becomes slightly longer (X-ray$_{av}$: 1.305 Å; DFT: 1.307 Å) and the N1'-C1' slightly shorter (X-ray$_{av}$: 1.276 Å; DFT: 1.298 Å) compared to the N1-C1 bond (X-ray$_{av}$: 1.291 Å; DFT: 1.299 Å) in the BG complex. This alteration is also observed in the computed complex, although the decrease in the N1'-C1' bond is only marginal. The asymmetrical nature of the ligand is also noticeable in different Cu-N bond distances of Cu-N1 1.942 Å and Cu-N1' 1.929 Å, surprisingly the DFT computed Cu-N bond distances show an opposite trend with 1.973 Å and 1.980 Å, which might be due to crystal packing effects compared to the gas-phase computed, single-molecule structure. However, the other bond distances are in excellent agreement.

The two crystal structures $Cu^{II}(Metf\text{-}H)_2 \cdot H_2O$ (ETOFOI)[65] and $Cu(Metf\text{-}H)_2 \cdot 8H_2O$ (EFIXUM)[64] were synthesized under basic conditions. The ETOFOI structure complex contains two $Cu^{II}(Metf\text{-}H)_2$ molecules in the unit cell with ETOFOI-A resembling the $Cu^{II}(BG\text{-}H)_2$ more closely than ETOFOI-B and EFIXUM. The best agreement with the DFT optimized $Cu(Metf\text{-}H)_2$ structure is also with ETOFOI-A. The lengthened N1-C1 and N1'-C1' double bond is particularly well reproduced by the B3LYP optimized structure.

Surprisingly, in EFIXUM and ETOFOI-B hardly any increase in the N1-C1 bond and decrease in the C1-N2 bond is observed, which most likely is due to strong H-bonding of crystal water in the proximity of N2. Two crystal waters are close two N2(-) in EFIXUM at a distance of 2.86 Å and 2.91 Å (N2-O distance), whereas one water is found in ETOFOI-B to be 2.84 Å away from N2(-).

Overall, the crystal structures of the neutral complex $Cu^{II}(Metf\text{-}H)_2$ indicate the possibility of the formation of stable Cu^{II} complex with deprotonated metformin at basic conditions.

TABLE 2

Only one crystal structure for the homoleptic PDI complex is known.[66] The Cu-N bond 1.956 Å in the $[Cu^{II}(PDI)_2]^{2+}$ complex is slightly longer than in the BG complex 1.943 Å, which is also observed in the computed structure with 1.999 Å compared to 1.980 Å, for PDI and BG respectively. In contrast to the BG complexes the C1-C2 bond (1.501 Å) in the PDI complex is much longer compared to the C1-N2 bond (1.373 Å) in $[Cu^{II}(BG)_2]^{2+}$ and closer to a pure single C-C bond than a double bond.

Intrigued by this long C1-C2 bond we calculated the rotational barrier of the free, neutral ligand of 2.42 kcal/mol for PDI and 18.20 kcal/mol for BG. The much higher rotational barrier for BG gives an indication about the strength of the conjugation of the N2 lone pair into the adjacent N1-C1 double bond.

TABLE 3

B. Binding Energies of $Cu^{I/II}$ Complexes

The binding energies that are presented in Table 2 were computed in two different ways. The interaction energy ΔE_{int} corresponds to the binding energy of the Cu-centre or CuOH fragment with the ligand in its geometry found in the optimized complex structure. On the other hand, the binding free energy ΔG is determined using the lowest energy tautomer and conformer of the ligands. The negative ΔG is equal to the dissociation energy D_e. The difference between the energy of the ligand in its complex geometry and its lowest tautomer and conformer is called preparation energy ΔE_{prep}.

We have computed binding energies for Cu^{I} and Cu^{II} complexes of the mono-L complexes, the homoleptic, bis-L complexes and the mixed $[Cu^{I/II}(OH)(L)]^{0/+}$ complexes. The latter is particular important in aqueous media as this is the major Cu^{II}-BG species at physiological pH in most biological compartments. We also calculated the complexes with deprotonated ligands as this might become important at higher physiological pH, occurring for example inside the mitochondria.

TABLE 4

Firstly, the $[Cu^{I/II}(L)]^{+/2+}$ complexes are discussed. Among all ligands Metf shows the strongest interaction energy with Cu^{I}, however, due to lower ΔE_{prep} PDI forms the strongest $[Cu^{I}(L)]^{+}$ complex. Interestingly, for BG and PDI ΔE_{int} is almost equal. En binds around 25-30 kcal/mol weaker to Cu^{I} compared to the other ligands, but D_e is only 6-16 kcal weaker, which as well is due to a small preparation energy. The weaker binding of en is due to the lack of π-backbonding, and also larger steric strain as en forms a 5-membered metallacycle compared to the 6-membered metallacycle of the BG, Metf and PDI-Cu complexes.

FIGURE 4

The Cu^{II} complexes for BG, Metf and PDI are more than 200 kcal/mol more stable than the Cu^{I} complex which is due to stronger Coulomb and orbital interactions. Whereas the en complex does not receive as strong a stabilisation compared to the other ligands. This could be due to two factors, the σ-bonding with the N lone pair is smaller in the sp^3 hybrid N compared to the slightly

larger sp^2 hybid lone pair with more s-character. The other factor, although this plays a minor role, is the possibility of the occupied ligand π-orbitals donating electron density towards the Cu-d^9 center. Overall, Metf binds strongest, however, the D_e of PDI is only 3.4 kcal/mol lower.

Secondly, we will consider the homoleptic $[Cu^{I/II}(L)_2]^{+/2+}$ complexes. For BG, Metf and PDI complexes we observe similar trends as in the mono-complexes, with an even stronger stabilisation for PDI compared to BG and Metf due to a much larger ΔE_{prep} for the latter ones. We also include trien in this group of complexes. Obviously due to its tetradentate, chelating properties it surpasses BG, Metf and PDI at equal molarity, however, we are more interested in its binding properties in comparison to copper-ligand complexes with a saturated copper ligand sphere. Trien has almost the same ΔE_{int} than en, but a larger D_e due to entropic effects by 5 kcal/mol with Cu^I and by ~10 kcal/mol with Cu^{II} which agrees with the experimentally observed stronger stabilisation of trien with Cu^{II}.

Next we will investigate the binding of BG, Metf, PDI and en in a mixed complex with Cu(OH), where OH is a stronger ligand than the neutral, bidentate ligands. The Cu^I cation forms a strong bond with the hydroxide anion, which results in weak binding of a second, non-anionic ligand. Here we observe a surprising order for the Cu^I complexes, PDI forms the strongest mixed complexes, en follows as the second strongest, then BG and Metf forms the weakest complex. The differences between the ligands is again mainly due to the larger ΔE_{prep} for BG and Metf compared to low ΔE_{prep} for PDI and en.

The mixed $Cu^{II}(OH)(L)$ complexes are slightly stronger than the $Cu^I(L)$ complexes, with very similar trends and similar stabilities for BG, Metf and PDI.

In addition to the complexes with neutral ligands we have also calculated the binding energies for the deprotonated BG-H, Metf-H and PDI-H. It is important to point out here that at higher pH

BG and Metf can be deprotonated in aqueous medium, whereas PDI, even when in a metal complex which lowers its pKa, will only be deprotonated above pH 14 in non-aqueous medium as the methylene group in PDI cannot be deprotonated by bases in aqueous media.

These anionic ligands bind much stronger than the neutral counterparts as they have much larger ionic bonding contributions than the neutral ligands. Also the Cu^{II} complexes receive an even stronger stabilization than the Cu^{I} complexes. This could indicate an easier oxidation compared to the neutral ligands when a Cu^{I} ion is extracted from a protein by Metf-H. In addition, these deprotonated forms of the biguanides alone might be a strong enough ligand to extract Cu^{I} from proteins with thiolate ligands. This modelling indicates that any copper-dependent effects of the drug may be restricted to or most prominent in the mitochondria and other compartments in the body where physiological pH is above the typical range, allowing deprotonation of the drug. Such pH-dependent activation or priming could potentially explain why metformin is almost invariably found in the biological literature to act on the mitochondria, with very few effects reported in other cellular compartments.

C. Electronic Properties

To gain a deeper understanding about the biguanide type ligands compared to the PDI we take a look at the molecular orbitals (MO) of these ligands in their geometry in a complex, see Figure 4. For simplicity we will concentrate on the π-orbitals and the MOs with the N1 lone pairs.

The lowest lying MOs with π-character in BG and PDI are the MO-19. PDI, which is not planar, still shows a π-like plane with one σ-C2-H bond above and the other σ-C2-H bond mixing with the N1-C1 double bond plus contribution from the N3 lone pairs. The MO-19 in BG is a mix of π and σ character. The lone pairs of N2 and N3 are mixing with the p_z AO of the sp^2

hybridized C1, plus σ-character from the N1-H bond. For BG the MO-21 looks very similar to the MO-19 with σ- and π-character, except that it is the negative combination of the AOs and therefore higher in energy. The MO-21 in PDI only shows σ-character, which explains the much lower rotational barrier for PDI compared to BG. The MO-22 is basically the same for both molecules. MO-23 in BG is a pure combination of N2 and N3 lone pairs, whereas in PDI as there is no lone pair on C2 this MO is a mix of π-MO with contributions from the N1-C1 double bonds and the N3 lone pairs plus out-of plane C2-H σ-bond character. MO-24 is the positive combination of the N1 lone pairs which is responsible for bonding to the empty 4s AO of Cu. The next two MOs 25 and 26 are identical for BG and PDI and are pure π-MOs. The HOMO, MO-27, is the negative combination of the N1 lone pairs and donate electron density into the empty 4p AO of Cu. These MOs show that the electron density on N1 is very similar in BG and PDI which explains the strong similarities in the observed binding energies for these ligands with Cu.

To emphasise this point we calculated the NBO charges for the $[Cu(L)]^{2+}$ complexes, Table 3. The charge on Cu decreases from +1.87, +1.84 to +1.80 for BG, PDI and en, respectively. This is coincident with decreasing negative charge on the ligand nitrogens N1 of these ligands from -0.87, -0.84 to -0.80. Figure 2 illustrates the possible orbital interactions for the sp^2-type N in BG, Metf and PDI compared to the sp^3-type N in en and trien. The former ones are capable of stronger bonds due to σ-donation while at the same time receiving electron density from the metal centre via π-backdonation, these two types of bonding have a synergistic effect and reinforce each other. On the other hand the pure σ-donor ligands en and trien cannot accept electron density in π-MOs, which results in weaker binding. The small difference between BG

and PDI can either be due to slightly larger σ-donation or smaller π-backdonation in PDI or a combination of both.

TABLE 5

D. ESP Maps

The electrostatic potential (ESP) maps for BG and PDI in their neutral forms are presented in Figure 5. Interestingly, the PDI-A shows a slightly more negative potential around the N1 atoms which will form coordination bonds toward Cu. This means that PDI is a slightly stronger Lewis base than BG-A and is consistent with our findings that the PDI has a larger ΔE_{int}. It has to be pointed out here that the presented structure PDI-A is not a minimum structure and therefore not stable in nature; however, this is the conformation that will bind to a metal center in a bidentate binding mode. BG-A on the other hand is a minimum structure, which also is in one sense surprising as the two N1 lone pairs should strongly repel each other, however, it seems that the p-stabilisation as shown by the MOs exceeds the steric repulsion. Also the methylene moiety causes a greater part of PDI-A to be hydrophobic compared to BG-A, which could be important in terms of molecular recognition when binding to a Cu centre of a protein. Therefore, not only does PDI cause greater steric hindrance due to its lack of planarity but also introduces repulsive or at least weaker interactions with H-bond acceptors.

FIGURE 5

The PDI-B represents the lowest energy conformer of the neutral PDI. An internal H-bond in PDI-B results in a very weak hydrophilicity, with strong, large areas that can be described as lipophilic. In contrast the BG-B, which is not the lowest tautomer of BG**,** shows much more pronounced negative and positive moieties which results in stronger H-bond donor and acceptor properties than PDI-B. This is suggestive evidence that PDI may be able to penetrate cell membranes, whereas BG and Metf need to be taken up via transmembrane transporters.

The lowest energy conformer and tautomer of BG-C does not show as strong Lewis acid or basic sites compared to BG-B, however, there are also fewer hydrophobic areas above the molecules plane which means that solvation and stabilisation due to H-bonding can be stronger not only on the edges of the molecules but also along the molecular plane.

DISCUSSION

In the presented study we find that the biologically observed differences between neutral biguanide compounds (BG and Metf) and PDI cannot be explained by different Cu-binding energies. These ligands are electronically too similar and the substitution of the secondary amine to methylene has no negative effect on the complex formation via the N1 nitrogens for PDI. However, the secondary amine of biguanides can be deprotonated in aqueous medium as the pKa value is reduced when BG or Metf are coordinated to $Cu^{I/II}$. These anions form much stronger complexes compared to their neutral form. It is known that the mitochondrial matrix pH is higher than normal cellular or serum pH. Inside the mitochondria it is possible that the equilibrium is shifted towards the $Cu^{I/II}$(Metf-H) complex. Extraction of Cu^{I} ions from proteins is possible and subsequent oxidation to Cu^{II} would remove the redox active Cu^{I} ions from the mitochondria. This

suggests that metformin could act in cells at least in part as a copper-binding prodrug, becoming activated by elevated mitochondrial pH. This is consistent with the strong emphasis on mitochondrial effects of this drug in the biological literature. In addition, this explains the differences between mitochondrial responses to metformin and PDI, as the latter agent only becomes deprotonated at much higher pH. There is a possibility that high binding affinities of Metf-H to copper could significantly affect the mitochondrial copper pool, which would probably have an impact on metal homeostasis of other metals and lead to mis-metallation of important metalloproteins.[67] Redox properties of such copper complexes may interfere with the sensitive redox chemistries occurring inside the cell, such as the mitochondrial electron transport chain.

Furthermore, ESP maps show that molecular recognition processes, which are copper-independent, could play a vital role in explaining the different drug properties of biguanides and PDI. Further work will establish if the much stronger hydrophilicity of BG facilitates its mitochondrial activity. On the other hand, we showed higher lipophilicity of PDI, which might enable it to penetrate cell membranes without relying on membrane transport proteins.

In summary, these calculations clearly demonstrate that metformin is a pH-sensitive copper-binding agent with a pK_a within the physiological pH range and a strongly hydrophilic character. Together, these properties of metformin distinguish it from the other copper-binding agents we have studied and they are also likely to account for many of the biological/therapeutic responses to the drug.

ASSOCIATED CONTENT

Supporting Information. Optimized geometries and corresponding energies for Table 1 and Table 2. This material is available free of charge via the Internet at http://pubs.acs.org.

AUTHOR INFORMATION

Corresponding Author

* Phone: +44(0)131 451 8035. E-mail: m.j.paterson@hw.ac.uk

Author Contributions

The manuscript was written through contributions of all authors. All authors have given approval to the final version of the manuscript.

REFERENCES

1. Danaei, G., Finucane, M. M., Lu, Y., Singh, G. M., Cowan, M. J., Paciorek, C. J., Lin, J. K., Farzadfar, F., Khang, Y.-H., Stevens, G. A., Rao, M., Ali, M. K., Riley, L. M., Robinson, C. A., and Ezzati, M. (2011) National, regional, and global trends in fasting plasma glucose and diabetes prevalence since 1980: Systematic analysis of health examination surveys and epidemiological studies with 370 country-years and 2·7 million participants, *The Lancet 378*, 31-40.
2. Mathers, C. D., and Loncar, D. (2006) Projections of global mortality and burden of disease from 2002 to 2030, *PLoS Med. 3*.
3. Rena, G., Pearson, E. R., and Sakamoto, K. (2013) Molecular mechanism of action of metformin: old or new insights?, *Diabetologia 56*, 1898-1906.

4. El-Mir, M. Y., Nogueira, V., Fontaine, E., Averet, N., Rigoulet, M., and Leverve, X. (2000) Dimethylbiguanide inhibits cell respiration via an indirect effect targeted on the respiratory chain complex I, *J. Biol. Chem. 275*, 223-228.

5. Owen, M. R., Doran, E., and Halestrap, A. P. (2000) Evidence that metformin exerts its anti-diabetic effects through inhibition of complex 1 of the mitochondrial respiratory chain, *Biochem. J. 348*, 607-614.

6. Camakaris, J., Voskoboinik, I., and Mercer, J. F. (1999) Molecular mechanisms of copper homeostasis, *Biochem. Biophys. Res. Commun. 261*, 225-232.

7. Linder, M. C., and HazeghAzam, M. (1996) Copper biochemistry and molecular biology, *Am. J. Clin. Nutr. 63*, S797-S811.

8. Olivares, M., and Uauy, R. (1996) Copper as an essential nutrient, *Am. J. Clin. Nutr. 63*, S791-S796.

9. Xu, W., Barrientos, T., and Andrews, Nancy C. (2013) Iron and Copper in Mitochondrial Diseases, *Cell Metab. 17*, 319-328.

10. Kaler, S. G., Buist, N. R. M., Holmes, C. S., Goldstein, D. S., Miller, R. C., and Gahl, W. A. (1995) Early copper therapy in classic Menkes disease patients with a novel splicing mutation, *Ann. Neurol. 38*, 921-928.

11. Madsen, E., and Gitlin, J. D. (2007) Copper deficiency, *Curr. Opin. Gastroenterol. 23*, 187-192.

12. Scheinberg, I. H., and Sternlieb, I. (1996) Wilson disease and idiopathic copper toxicosis, *Am. J. Clin. Nutr. 63*, S842-S845.

13. Christen, Y. (2000) Oxidative stress and Alzheimer disease, *Am. J. Clin. Nutr. 71*, 621S-629S.

14. Cobb, N. J., and Surewicz, W. K. (2009) Prion diseases and their biochemical mechanisms, *Biochemistry 48*, 2574-2585.

15. Eskici, G., and Axelsen, P. H. (2012) Copper and oxidative stress in the pathogenesis of Alzheimer's disease, *Biochemistry 51*, 6289-6311.

16. Masad, A., Hayes, L., Tabner, B. J., Turnbull, S., Cooper, L. J., Fullwood, N. J., German, M. J., Kametani, F., El-Agnaf, O. M. A., and Allsop, D. (2007) Copper-mediated formation of hydrogen peroxide from the amylin peptide: A novel mechanism for degeneration of islet cells in type-2 diabetes mellitus?, *FEBS Lett. 581*, 3489-3493.

17. Gybina, A. A., and Prohaska, J. R. (2008) Fructose-2,6-bisphosphate is lower in copper deficient rat cerebellum despite higher content of phosphorylated AMP-activated protein, *Exp. Biol. Med. 233*, 1262-1270.

18. Gybina, A. A., and Prohaska, J. R. (2008) Copper deficiency results in AMP-activated protein kinase activation and acetylCoA carboxylase phosphorylation in rat cerebellum, *Brain Res. 1204*, 69-76.

19. Tanaka, A., Kaneto, H., Miyatsuka, T., Yamamoto, K., Yoshiuchi, K., Yamasaki, Y., Shimomura, I., Matsuoka, T. A., and Matsuhisa, M. (2009) Role of copper ion in the pathogenesis of type 2 diabetes, *Endocr. J. 56*, 699-706.

20. Dosa, M. D., Hangan, L. T., Crauciuc, E., Gales, C., and Nechifor, M. (2011) Influence of therapy with metformin on the concentration of certain divalent cations in patients with non-insulin-dependent diabetes mellitus, *Biol. Trace Elem. Res. 142*, 36-46.

21. Logie, L., Harthill, J., Patel, K., Bacon, S., Hamilton, D. L., Macrae, K., McDougall, G., Wang, H.-H., Xue, L., Jiang, H., Sakamoto, K., Prescott, A. R., and Rena, G. (2012) Cellular responses to the metal-binding properties of metformin, *Diabetes 61*, 1423-1433.

22. Boal, A. K., and Rosenzweig, A. C. (2009) Structural biology of copper trafficking, *Chem. Rev. 109*, 4760-4779.

23. Bertini, I., and Rosato, A. (2003) Bioinorganic chemistry in the postgenomic era, *Proc. Natl. Acad. Sci. U. S. A. 100*, 3601-3604.

24. Puig, S., and Thiele, D. J. (2002) Molecular mechanisms of copper uptake and distribution, *Curr. Opin. Chem. Biol. 6*, 171-180.

25. Rubino, J. T., and Franz, K. J. (2012) Coordination chemistry of copper proteins: How nature handles a toxic cargo for essential function, *J. Inorg. Biochem. 107*, 129-143.

26. Nose, Y., Rees, E. M., and Thiele, D. J. (2006) Structure of the Ctr1 copper trans'PORE'ter reveals novel architecture, *Trends Biochem. Sci. 31*, 604-607.

27. Abajian, C., Yatsunyk, L. A., Ramirez, B. E., and Rosenzweig, A. C. (2004) Yeast Cox17 solution structure and copper(I) binding, *J. Biol. Chem. 279*, 53584-53592.

28. Horn, D., and Barrientos, A. (2008) Mitochondrial copper metabolism and delivery to cytochrome c oxidase, *IUBMB Life 60*, 421-429.

29. Wang, Y. F., Hodgkinson, V., Zhu, S., Weisman, G. A., and Petris, M. J. (2011) Advances in the understanding of mammalian copper transporters, *Adv Nutr 2*, 129-137.

30. Pearson, R. G. (1963) Hard and soft acids and bases, *J. Am. Chem. Soc. 85*, 3533-3539.

31. Pearson, R. G. (1968) Hard and soft acids and bases, HSAB, part I: Fundamental principles, *J. Chem. Educ. 45*, 581-587.

32. Pearson, R. G. (1968) Hard and soft acids and bases, HSAB, part II: Underlying theories, *J. Chem. Educ. 45*, 643-648.

33. Parr, R. G., and Pearson, R. G. (1983) Absolute hardness: Companion parameter to absolute electronegativity, *J. Am. Chem. Soc. 105*, 7512-7516.

34. Huheey, J. E., Keiter, E. A., and Keiter, R. L. (1993) *Inorganic chemistry: Principles of structure and reactivity*, HaperCollins College Publisher, New York.

35. Solomon, E. I., Szilagyi, R. K., DeBeer George, S., and Basumallick, L. (2004) Electronic structures of metal sites in proteins and models: Contributions to function in blue copper proteins, *Chem. Rev. 104*, 419-458.

36. Feldman, J., McLain, S. J., Parthasarathy, A., Marshall, W. J., Calabrese, J. C., and Arthur, S. D. (1997) Electrophilic metal precursors and a beta-diimine ligand for nickel(II)- and palladium(II)-catalyzed ethylene polymerizations, *Organometallics 16*, 1514-1516.

37. Holland, P. L., and Tolman, W. B. (1999) Three-coordinate Cu(II) complexes: Structural models of trigonal-planar type 1 copper protein active sites, *J. Am. Chem. Soc. 121*, 7270-7271.

38. Randall, D. W., George, S. D., Holland, P. L., Hedman, B., Hodgson, K. O., Tolman, W. B., and Solomon, E. I. (2000) Spectroscopic and electronic structural studies of blue copper model complexes. 2. Comparison of three- and four-coordinate Cu(II)-thiolate complexes and fungal laccase, *J. Am. Chem. Soc. 122*, 11632-11648.

39. Bharatam, P. V., Patel, D. S., and Iqbal, P. (2005) Pharmacophoric features of biguanide derivatives: An electronic and structural analysis, *J. Med. Chem. 48*, 7615-7622.

40. Dias, H. V. R., and Singh, S. (2004) Silver(I) complexes of a sterically demanding fluorinated triazapentadienyl ligand $[N\{(C_3F_7)C(Dipp)N\}(_2)]^-$ (Dipp 2,6-diisopropylphenyl), *Inorg. Chem. 43*, 7396-7402.

41. Flores, J. A., and Dias, H. V. R. (2008) Gold(I) ethylene and copper(I) ethylene complexes supported by a polyhalogenated triazapentadienyl ligand, *Inorg. Chem. 47*, 4448-4450.

42. Kopylovich, M. N., and Pombeiro, A. J. L. (2011) Coordination chemistry of 1,3,5-triazapentadienes, *Coord. Chem. Rev. 255*, 339-355.

43. Randall, D. W., George, S. D., Holland, P. L., Hedman, B., Hodgson, K. O., Tolman, W. B., and Solomon, E. I. (2000) Spectroscopic and electronic structural studies of blue copper model complexes. 2. Comparison of three- and four-coordinate Cu(II)-thiolate complexes and fungal laccase, *J. Am. Chem. Soc. 122*, 11632-11648.

44. Barman, T. R., and Mukherjee, G. N. (2006) Mixed-ligand complex formation equilibria of Cu-II with biguanide in presence of glycine as the auxiliary ligand, *J. Chem. Sci. (Bangalore, India) 118*, 411-418.

45. Barman, T. R., and Mukherjee, G. N. (2009) Coordination equilibria of mixed ligand complexes of Cu-II with glycylglycine and biguanide, *Indian J Chem A 48*, 38-44.

46. Olar, R., Badea, M., Marinescu, D., Chifiriuc, C. M., Bleotu, C., Grecu, M. N., Iorgulescu, E. E., Bucur, M., Lazar, V., and Finaru, A. (2010) Prospects for new antimicrobials based on N,N-dimethylbiguanide complexes as effective agents on both planktonic and adhered microbial strains, *Eur. J. Med. Chem. 45*, 2868-2875.

47. Olar, R., Badea, M., Marinescu, D., Chifiriuc, M.-C., Bleotu, C., Grecu, M. N., Iorgulescu, E.-E., and Lazar, V. (2010) N,N-dimethylbiguanide complexes displaying low cytotoxicity as potential large spectrum antimicrobial agents, *Eur. J. Med. Chem. 45*, 3027-3034.

48. Solomon, E. I., Szilagyi, R. K., George, S. D., and Basumallick, L. (2004) Electronic structures of metal sites in proteins and models: Contributions to function in blue copper proteins, *Chem. Rev. 104*, 419-458.

49. Becke, A. D. (1993) Density-functional thermochemistry. III. The role of exact exchange, *J. Chem. Phys. 98*, 5648-5652.

50. Stephens, P. J., Devlin, F. J., Chabalowski, C. F., and Frisch, M. J. (1994) Ab initio calculation of vibrational absorption and circular dichroism spectra using density functional force fields, *J. Phys. Chem. 98*, 11623-11627.

51. Becke, A. D. (1988) Density-functional exchange-energy approximation with correct asymptotic behavior, *Phys. Rev. A 38*, 3098-3100.

52. Vosko, S. H., Wilk, L., and Nusair, M. (1980) Accurate spin-dependent electron liquid correlation energies for local spin density calculations: a critical analysis, *Can. J. Phys. 58*, 1200-1211.

53. Lee, C., Yang, W., and Parr, R. G. (1988) Development of the Colle-Salvetti correlation-energy formula into a functional of the electron density, *Phys. Rev. B 37*, 785-789.

54. Rappoport, D., and Furche, F. (2010) Property-optimized Gaussian basis sets for molecular response calculations, *J. Chem. Phys. 133*, 134105-134111.

55. Frisch, M. J., Trucks, G. W., Schlegel, H. B., Scuseria, G. E., Robb, M. A., Cheeseman, J. R., Scalmani, G., Barone, V., Mennucci, B., Petersson, G. A., Nakatsuji, H., Caricato, M., Li, X., Hratchian, H. P., Izmaylov, A. F., Bloino, J., Zheng, G., Sonnenberg, J. L., Hada, M., Ehara, M., Toyota, K., Fukuda, R., Hasegawa, J., Ishida, M., Nakajima, T., Honda, Y., Kitao, O., Nakai, H., Vreven, T., Montgomery, J., J. A., Peralta, J. E., Ogliaro, F., Bearpark, M., Heyd, J. J., Brothers, E., Kudin, K. N., Staroverov, V. N.,

Kobayashi, R., Normand, J., Raghavachari, K., Rendell, A., Burant, J. C., Iyengar, S. S., Tomasi, J., Cossi, M., Rega, N., Millam, J. M., Klene, M., Knox, J. E., Cross, J. B., Bakken, V., Adamo, C., Jaramillo, J., Gomperts, R., Stratmann, R. E., Yazyev, O., Austin, A. J., Cammi, R., Pomelli, C., Ochterski, J. W., Martin, R. L., Morokuma, K., Zakrzewski, V. G., Voth, G. A., Salvador, P., Dannenberg, J. J., Dapprich, S., Daniels, A. D., Farkas, Ö., Foresman, J. B., Ortiz, J. V., Cioslowski, J., and Fox, D. J. Gaussian 09 Revision A.02, Gaussian, Inc., Wallingford CT, 2009.

56. Perdew, J. P. (1986) Density-functional approximation for the correlation energy of the inhomogeneous electron gas, *Phys. Rev. B 33*, 8822-8824.

57. Zhao, Y., and Truhlar, D. (2008) The M06 suite of density functionals for main group thermochemistry, thermochemical kinetics, noncovalent interactions, excited states, and transition elements: Two new functionals and systematic testing of four M06-class functionals and 12 other functionals, *Theor. Chem. Acc. 120*, 215-241.

58. Zhao, Y., and Truhlar, D. G. (2006) A new local density functional for main-group thermochemistry, transition metal bonding, thermochemical kinetics, and noncovalent interactions, *J. Chem. Phys. 125*, 194101-194118.

59. Glendening, E. D., Reed, A. E., Carpenter, J. E., and Weinhold, F. NBO Version 3.1.

60. Coghi, L., Lanfranchi, M., Pelizzi, G., and Tarasconi, P. (1978) Structural researches on the chelating behaviour of the biguanide ligand. The crystal structures of $Co(C_2H_6N_5)_3 \cdot 2H_2O$ and $Cu(C_2H_7N_5)_2CO_3 \cdot 4H_20$, *Transition Met. Chem. (Dordrecht, Neth.) 3*, 69-76.

61. Hota, S. K., Saha, C. R., and Pritzkow, H. (1984) Syntheses and properties of some 5-coordinate and 6-coordinate copper(II) complexes with acetylacetonate and the structural characterization of a biguanide-acetylacetonate double salt, *J. Coord. Chem. 13*, 131-142.

62. Kennard, C. H. L., Smith, G., and O'Reilly, E. J. (1983) The crystal and molecular structure of bis(biguanide)copper(II) chloride dihydrate, *Inorg. Chim. Acta 77*, L113-L115.

63. Su, Y. L., Lu, L. P., Li, X. M., and Zhu, M. L. (2005) Bis(biguanido-κ^2-N,N')copper(II) dihydrate, *Acta Crystallogr., Sect. E: Struct. Rep. Online 61*, m910-m912.

64. Zhu, M., Lu, L., Yang, P., and Jin, X. (2002) Bis(1,1-dimethylbiguanido)copper(II) octahydrate, *Acta Crystallogr., Sect. E: Struct. Rep. Online 58*, m217-m219.

65. Lu, L. P., Yang, P., Qin, S. D., and Zhu, M. L. (2004) Bis[1,1-dimethylbiguanide(1-)-κ^2N^2,N^5]copper(II) monohydrate, *Acta Crystallogr., Sect. C: Cryst. Struct. Commun. 60*, m219-m220.

66. Schwarzenbach, D., and Schmelczer, R. (1978) Comparison of an OD and an ordered structure of nickel and copper malondiamidine complexes, *Acta Crystallogr., Sect. B: Struct. Sci. 34*, 1827-1833.

67. Pierrel, F., Cobine, P. A., and Winge, D. R. (2007) Metal ion availability in mitochondria, *Biometals 20*, 675-682.

68. Viossat, B., Tomas, A., and Dung, N.-H. (1995) L'hydrogenocarbonate de Bis(N,N-dimethylbiguanide) Cuivre(II), $[Cu(C_4H_{11}N_5)_2]_2HCO_3$, *Acta Crystallogr., Sect. C: Cryst. Struct. Commun. 51*, 213-215.

69. Lemoine, P., Chiadmi, M., Bissery, V., Tomas, A., and Viossat, E. (1996) Les Composés de la Metformine avec les Ions Co(II), Cu(II) et Ni(II), *Acta Crystallogr., Sect. C: Cryst. Struct. Commun. 52*, 1430-1436.

FIGURES

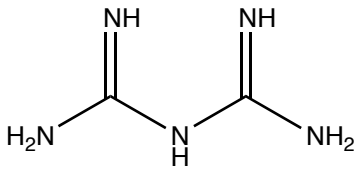

biguanide
(BG)

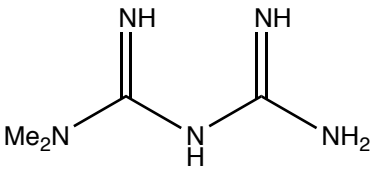

1,1'-dimethylbiguanide
(metformin, Metf)

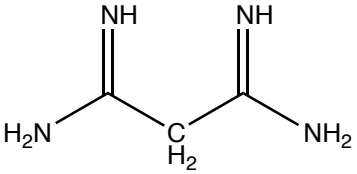

propanediimidamide
(PDI)

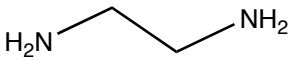

ethylenediamine
(en)

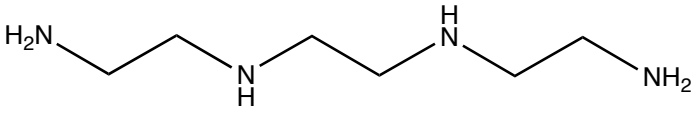

triethylenetetramine
(trien)

Figure 1. Compounds used as ligands

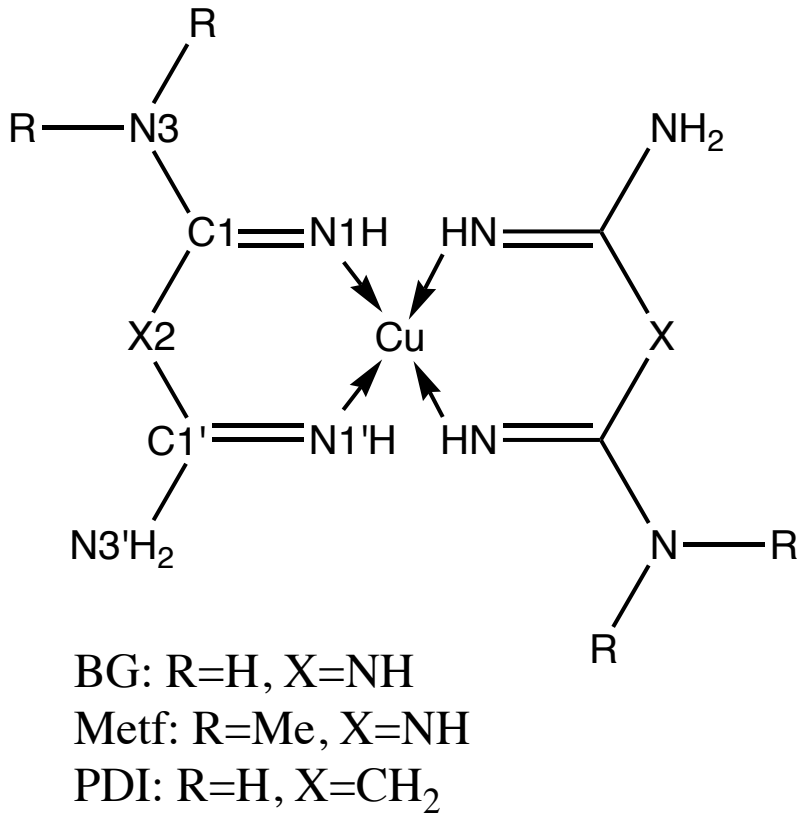

Figure 2. Numbering of atoms in X-ray and computed structures.

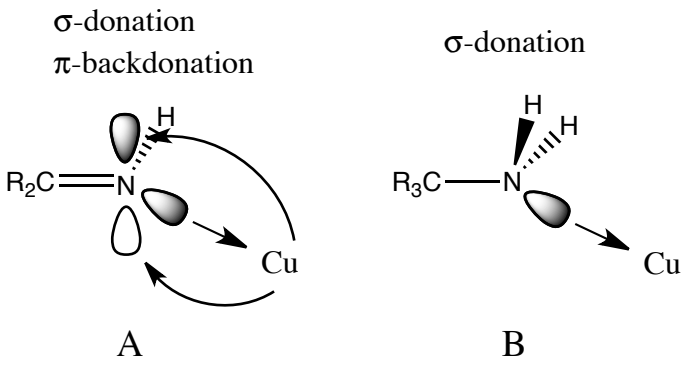

Figure 3. Schematic representation of possible orbital interactions Cu complexes with BG, Metf and PDI (A) and with en and trien (B)

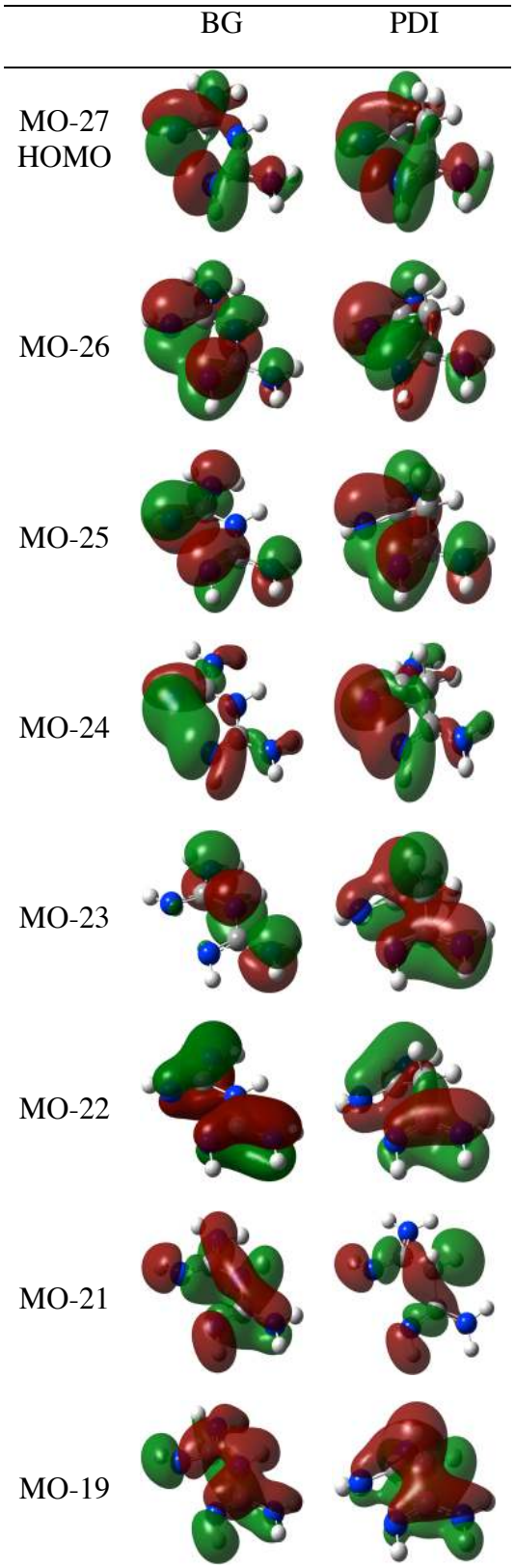

Figure 4. Molecular orbitals for BG and PDI

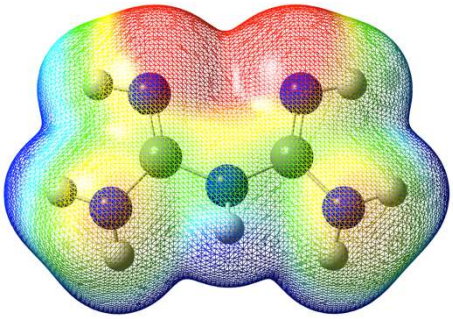

BG-A
+20.90 kcal/mol
(minimum)

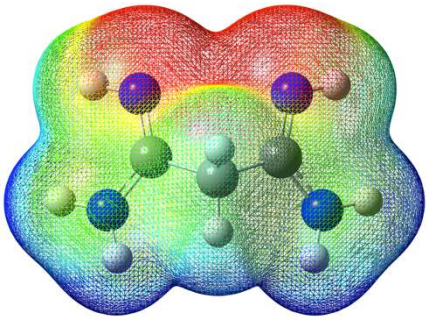

PDI-A
+16.18 kcal/mol
(no minimum)

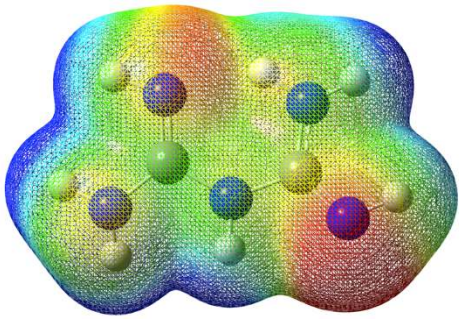

BG-B
+6.42 kcal/mol
(minimum)

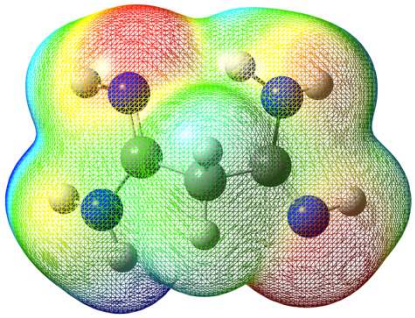

PDI-B
0.00 kcal/mol
(minimum)

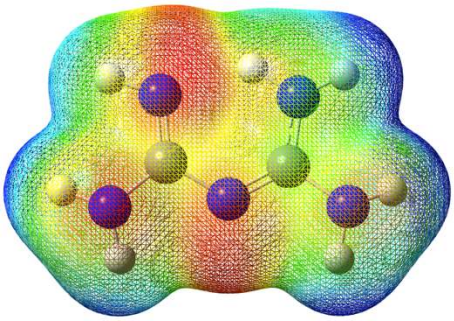

BG-C
+0.00 kcal/mol
(minimum)

Figure 5. Electrostatic potential maps for BG and PDI. Red negative, green neutral and blue positive ESP values.

TABLES.

Table 1. Comparison of critical bonds[†] (distance in Ångström) of $[Cu^{II}(BG)_2]X_{1,2}$ (X= CO_3^{2-}, Cl^-, $[Cu^{II}(C_5H_7O_2)(Cl)]^-$) and $Cu^{II}(BG\text{-}H)_2$ crystal structures and computed $[Cu^{II}(BG/BG\text{-}H)_2]^{2+/0}$ complexes.

BG	CSD code	X	Cu-N	N1-C1	C1-N2	C1-N3
X-ray	BGCUCB[60]	CO_3^{2-}	1.951	1.296	1.374	1.351
	COBMAH[61]	$[Cu^{II}(C_5H_7O_2)(Cl)]^-$	1.936	1.287	1.372	1.337
	ZZZDZQ01[62]	Cl^-	1.941	1.289	1.373	1.342
	Ø[‡]([Cu(BG)$_2$]$^{2+}$		*1.944*	*1.292*	*1.373*	*1.344*
	STD		*0.011*	*0.009*	*0.009*	*0.012*
	MUE		*0.023*	*0.016*	*0.017*	*0.018*
B3LYP	$[Cu(BG)_2]^{2+}$		1.980	1.299	1.383	1.344
X-ray	SAPFUL[63]	—	1.941	1.320	1.355	1.360
B3LYP	$Cu(BG\text{-}H)_2$		1.971	1.318	1.337	1.383

[†]Experimental bond lengths are averaged for each crystal structure (BGCUCB C_1-symmetry, COBMAH C_i symmetry and ZZZDZQ01 C_1 symmetry. [‡]Average of all $[Cu^{II}(BG)_2]X_{1,2}$ structures.

Table 2. Comparison of critical bond[†] (distance in Ångström) of $[Cu^{II}(Metf)_2]X_{1,2}$ (X= ClO_4^-, CO_3^{2-}, Cl^-) and $Cu^{II}(Metf\text{-}H)_2$ crystal structures and computed complexes.

Metf	CSD code	X	Cu-N1	Cu-N1'	N1-C1	N1'-C1'	C1-N2	C1'-N2	C1-N3	C1'-N3'
X-ray	AJUHUJ[47]	ClO_4^-	1.944	1.944	1.303	1.268	1.374	1.384	1.354	1.344
	HIBPOX[68]	CO_3^{2-}	1.931	1.920	1.305	1.282	1.364	1.393	1.342	1.322
	HIHDUX[69]	Cl^-	1.948	1.931	1.307	1.279	1.377	1.379	1.342	1.344
	Ø($[Cu(Metf)_2]^{2+}$)		*1.941*	*1.932*	*1.305*	*1.276*	*1.372*	*1.385*	*1.346*	*1.337*
	STD		*0.009*	*0.012*	*0.002*	*0.007*	*0.007*	*0.007*	*0.007*	*0.013*
	MUE		*0.010*	*0.012*	*0.002*	*0.008*	*0.008*	*0.008*	*0.008*	*0.015*
B3LYP	$[Cu(Metf)_2]^{2+}$		1.973	1.980	1.307	1.298	1.389	1.379	1.346	1.348
X-ray	EFIXUM[64]	—	1.943	1.921	1.312	1.306	1.372	1.350	1.365	1.386
	ETOFOI[65]-A[†]	—	1.938	1.928	1.324	1.320	1.358	1.350	1.368	1.371
	ETOFOI[65]-B[†]	—	1.950	1.923	1.315	1.310	1.371	1.342	1.357	1.391
	Ø($Cu(Metf\text{-}H)_2$)		*1.944*	*1.924*	*1.317*	*1.312*	*1.367*	*1.347*	*1.363*	*1.383*
	STD		*0.006*	*0.004*	*0.006*	*0.007*	*0.008*	*0.005*	*0.006*	*0.010*
	MUE		*0.006*	*0.004*	*0.007*	*0.008*	*0.009*	*0.005*	*0.006*	*0.012*
B3LYP	$Cu(Metf\text{-}H)_2$		1.970	1.967	1.323	1.320	1.343	1.332	1.383	1.388

[†]The unit cell of ETOFOI contains two $Cu(Metf\text{-}H)_2$ molecules.

Table 3. Comparison of critical structural parameters (bond distance in Ångström, angle in degrees) of $[Cu^{II}(PDI)_2][ClO_4]_2$ crystal structures and computed $[Cu^{II}(PDI/PDI\text{-}H)_2]^{2+/0}$ complexes.

PDI	**CSD code**	**X**	**Cu-N**	**N1-C1**	**C1-C2**	**C1-N3**	**∠N1-N2-C3-C2**[†]
X-ray	MALDOU[66]	ClO_4^-	1.956	1.288	1.501	1.332	21.6
B3LYP	$[Cu(PDI)_2]^{2+}$		1.999	1.297	1.514	1.336	22.1
	$[Cu(PDI\text{-}H)_2]^0$		1.976	1.321	1.403	1.394	1.4

Table 4. Binding energies of Cu complexes. B3LYP/Def2-TZVPD. Energies in kcal/mol.

		BG	Metf	PDI	en	trien
$[Cu^{I}(L)]^{+}$	ΔE_{int}	-119.77	-125.07	-120.74	-95.15	
	$\Delta G (=-D_e)$	-84.71	-87.45	-94.18	-78.60	
$[Cu^{II}(L)]^{2+}$	ΔE_{int}	-331.77	-347.81	-332.66	-270.92	
	$\Delta G (=-D_e)$	-286.23	-299.91	-296.49	-250.70	
$[Cu^{I}(L)_2]^{+}$	ΔE_{int}	-183.80	-187.80	-186.28	-154.32	-151.04
	$\Delta G (=-D_e)$	-105.97	-106.64	-124.85	-112.52	-117.58
$[Cu^{II}(L)_2]^{2+}$	ΔE_{int}	-489.52	-505.09	-488.51	-410.06	-409.90
	$\Delta G (=-D_e)$	-391.59	-402.19	-405.96	-355.32	-364.10
$[Cu^{I}(OH)(L)]$	ΔE_{int}	-50.88	-47.80	-51.05	-42.10	
	$\Delta G (=-D_e)$	-16.26	-12.02	-34.12	-24.60	
$[Cu^{II}(OH)(L)]^{+}$	ΔE_{int}	-138.25	-144.61	-138.73	-112.33	
	$\Delta G (=-D_e)$	-97.37	-101.23	-105.93	-88.99	
$[Cu^{I}(L\text{-}H)]$	ΔE_{int}	-229.86	-231.38	-234.86		
	$\Delta G (=-D_e)$	-200.71	-201.60	-203.80		
$[Cu^{II}(L\text{-}H)]^{+}$	ΔE_{int}	-555.26	-561.38	-566.70		

	ΔG (=-D_e)	-511.20	-518.40	-530.24
$[Cu^{I}(L\text{-}H)_2]^-$	ΔE_{int}	-353.80	-351.71	-359.31
	ΔG (=-D_e)	-220.55	-220.70	-218.21
$[Cu^{II}(L\text{-}H)_2]$	ΔE_{int}	-836.32	-837.06	-846.10
	ΔG (=-D_e)	-678.65	-680.45	-680.12

Table 5. NBO charges for $[Cu^{II}(L)]^{2+}$, L=BG, PDI and en.

	BG	PDI	EN
Cu^{II}	+1.38	+1.34	+1.30
N1	-0.87	-0.84	-0.80

For TOC graphic: